Received: 1 October 2023 | Revised: 5 February 2024 | Accepted: 18 March 2024

DOI: 10.1002/ese3.1745

ORIGINAL ARTICLE

Interface passivation using diketopyrrolopyrrole-oligothiophene copolymer to improve the performance of perovskite solar cells

Samuel Abicho[1,2,3,4] | **Bekele Hailegnaw**[5] | **Felix Mayr**[3] | **Munise Cobet**[3] | **Cigdem Yumusak**[3] | **Siraye Esubalew**[1] | **Teketel Yohannes**[6] | **Martin Kaltenbrunner**[5] | **Niyazi Serdar Sariciftci**[3] | **Markus Clark Scharber**[3] | **Getachew Adam Workneh**[1,2]

[1]Department of Industrial Chemistry, Addis Ababa Science and Technology University, Addis Ababa, Ethiopia

[2]Sustainable Energy Center of Excellence, Addis Ababa Science and Technology University, Addis Ababa, Ethiopia

[3]Linz Institute for Organic Solar Cells (LIOS)/Institute of Physical Chemistry, Johannes Kepler University, Linz, Austria

[4]Department of Chemistry, Hawassa University, Hawassa, Ethiopia

[5]Division of Soft Matter Physics and LIT Soft Materials Lab, Johannes Kepler University, Linz, Austria

[6]Department of Chemistry, Addis Ababa University, Addis Ababa, Ethiopia

Correspondence
Getachew Adam Workneh, Department of Industrial Chemistry, Addis Ababa Science and Technology University, P.O. Box 16417, Addis Ababa, Ethiopia.
Email: getachew.adam@aastu.edu.et

Funding information
We would like to acknowledge Erasmus+ KA107 (project number 2020-1-AT01-KA107-077800), Linz Institute for Organic Solar cells (LIOS), Johannes Kepeler University, Linz, Africa Uni-net and OeAD-GmbH – Austria's Agency for Education and Internationalization, Addis Ababa Science and Technology University, Hawassa University for their

Abstract

The unprecedented increase in power conversion efficiency (PCE) of low-cost organo-inorganic halide perovskite solar cells (OIHPSCs) toward its Shockley-Queisser limit intriguingly has prompted researchers to investigate the disadvantages of these devices. The issue of operational stability is the main hurdle challenging the way forward for commercialization. To address this, various engineering processes like composition, additives, anti-solvents, bulk and interface passivation, and deposition techniques have been widely applied to manage both extrinsic and intrinsic factors that induce degradation of the OIHPSCs. In this work, we employed interface passivation, which is an efficient approach to reduce nonradiative recombination. An ultrathin layer of electron donor diketopyrrolopyrrole-oligothiophene copolymer (DPP860) was applied as an interface passivator between the photoactive layer and [6,6]-phenyl C_{61} butyric acid methyl ester (PCBM). The role of the interface passivation on optoelectronic properties of the OIHPSCs was assessed using current density versus voltage (J-V) characteristics, photoluminescence spectroscopy and time-resolved photoluminescence spectroscopy. The findings show devices treated with DPP860 exhibit enhanced current density (J_{sc}) and fill factor, attributing for suppressed nonradiative recombination. Moreover, it shows relative improvement in the stability of the device. The results of this finding reveal that using oligothiophene copolymer can enhance the photovoltaic performance and the stability of inverted OIHPSCs in the ambient environment.

financial, materials and laboratory support

KEYWORDS

interface passivation, nonradiative recombination, organo-inorganic halide perovskite solar cells, power conversion efficiency, stability

1 | INTRODUCTION

Low-cost solar energy converting devices have a significant role in achieving the access to affordable clean energy goal of Sustainable Development. Cost lowering is mainly dependent on the processing cost of a solar cell. Nowadays, fast-growing and low-cost solution-processed OIHPSCs have drawn the attention of many researchers due to their high performance and flexibility to satisfy the strong energy demand.[1,2] This is ascribed to excellent optical and electrical characteristics, such as direct band gap, high light absorption coefficient, high charge carrier mobility, long charge carrier diffusion length, and long electron-hole recombination lifetime.[3–5] Even though their indoor performance is promising, they degrade in ambient conditions. Consequently, different strategies such as compositional, additive, interface, and passivation engineering and various deposition techniques have been widely used to overcome extrinsic and intrinsic factors which affect the performance and stability in the ambient environment.[6–10]

The communication barrier between different layers due to interface nonradiative recombination could have a substantial negative impact on the performance and stability of the OIHPSCs.[11] Thus, interface engineering using either organic or inorganic compounds has emerged as the promising approach to solve such issues to commercialize OIHPSCs.[12–14] This strategy could help to tune electronic properties, viz. energy level alignment,[15] form interface dipole,[16] passivate charge trapping centers (defects),[17] and prevent infiltration of moisture.[18] Thus, organic polymers that contain different functional groups like thiol, carbonyl, carboxyl, hydroxyl, ethers and amine, have dual effects. Prominently, they act as Lewis base additives to bind specifically with uncoordinated Pb^{2+} during OIHP solution formation.[19,20] They could also form hydrogen or halogen bonds with organic monocation or halides of the OIHP. Their integration as an additive retards the crystallization of lead halides (PbX_2) and facilitates the formation of a homogeneous solution.[21] As a result, the morphology of the OIHP thin films could be improved. Moreover, it improves the crystallinity and grain size of the film, and film coverage, which suppresses the formation of charge trap centers and hysteresis.[22] On the other hand, they passivate the bulk and interface defects which induce nonradiative recombination. This strategy has a substantial effect on preventing the diffusion of ions across a grain boundary and suppressing nonradiative recombination across the interface.[23]

The power conversion efficiency and stability of the OHHPSCs may be greatly increased by enhancing smoothness and surface coverage of the photoactive and charge transport layers. Solution-processed PCBM has been applied as the most common electron-transporting material in inverted (p-i-n) OIHPSCs. However; it is censured due to its low film coverage, low electron mobility, and conductivity.[24,25] In this work, diketopyrrolopyrrole-oligothiophene copolymer (DPP860),[26] is used as the interface passivator between OIHP and PCBM to mitigate the interface defects. The findings from dark current, photoluminescence (PL), time-resolved photoluminescence (TRPL), and intensity-modulated photovoltage (IMV) measurements show that nonradiative recombination is minimized due to passivation. Specifically, interface passivation using DPP860 unveil eminent improvement in short current density (J_{sc}) and fill factor of the fabricated OIHPSCs which is attributed to the contribution of DPP860 in facilitating electron injection from OIHP layer to PCBM. The results, which are extracted from the maximum power point tracking (MPPT) measurement, also indicate the enhancement of operational stability in the ambient environment for devices with interface passivation. This confirms DPP860 is a good candidate to minimize interfacial defects of OIHPSCs.

2 | EXPERIMENTAL DETAILS

2.1 | Materials and perovskite solution preparation

Methylamine (33 wt %, in absolute ethanol; Sigma Aldrich), hydroiodic acid (HI (aq), 57 wt %; Sigma Aldrich), diethyl ether (VWR Chemicals), and ethanol (absolute. MERCK) were used to synthesize and purify methylammonium iodide (MAI) according to the literature.[27] TiOx sol-gel is also synthesized based on the procedure reported by Park et al.[28] The solution of $MAPbI_3$ was prepared by mixing defined molar ratios of lead halides and methyl ammonium iodide in a 1:1:4 mol ratio of PbI_2, $PbCl_2$, and MAI, respectively.[29] Then, the

mixture of the precursors were dissolved in DMF containing 10.0% acetyl acetone (AA) as the solvent additive, and was stirred overnight at about 45°C.[30] Finally, the prepared solution was ready for device fabrication after filtering using a 0.45 μm polytetrafluoroethylene (PTFE) filter.

2.2 | Device fabrication

ITO-coated glass substrates were cleaned by using Hellmanex surfactant, deionized water, acetone, and isopropanol (IPA), respectively, for about 20 min of each step in an ultrasonic bath. The cleaned substrate was dried with nitrogen gas (N_2). PEDOT:PSS (Clevios PH1000) solution was prepared by adding 7% dimethyl sulfoxide (DMSO) and 0.7% Zonyl® FS-300 fluorosurfactant and it was mixed well to enhance the conductivity.[31] It was spin-coated as the hole transport layer (HTL) at 1250 and 2000 rpm for 45 s and annealed at 120°C for 15 min. The films were washed by IPA at 2000 rpm for 2 s and 4000 rpm for 10 s and annealed for 15 min at 120°C. After cooling the PEDOT:PSS films to room temperature, the filtered solution of perovskite ($MAPbI_3$) using 0.45 μm polytetrafluoroethylene (PTFE) filter was spin-coated at 1250 rpm for 17 s and 2000 rpm for 5 s on the top of the hole transport layer. The samples were kept on stand for 1 min before being transferred to the hot plate and annealed for 30 min at 110°C. Subsequently, different concentrations of diketopyrrolopyrrole-oligothiophene copolymer (DPP860) solution (0.3, 0.7, and 1.0 mg mL^{-1}) in chlorobenzene (CB) were prepared and spin-coated on top of the OIHP layer as capping layer at 5000 rpm for 30 s to find the optimal thickness. Then after, 20 mg mL^{-1} of PCBM solution in chlorobenzene and chloroform (1:1) volume ratio was spin-coated on top of the DPP860 thin layer as electron transport layer (ETL) at 1250 rpm for 16 s and 2000 rpm for 15 s. Henceforth, TiO_x sol-gel was spin-coated on the top of the ETL at 5000 rpm for 30 s and annealed at 107°C for 7 min as a buffer layer. All above procedures were carried out in an ambient environment and finally, inverted perovskite solar device configuration: (ITO/PEDOT:PSS/$MAPbI_3$/DPP860/PCBM/TiOx/Al) was completed by thermal evaporation of ~110 nm aluminum back contact.

2.3 | Characterization

The thickness of different layers was measured by the profilometer (Bruker Dektak.XT). Ossila Contact Angle Goniometer (L2004A1) were used to carry out the contact angle measurements of the OIHP films at room temperature using 18 MΩ ultra-pure water.

Fourier transform infrared spectroscopy (FTIR) spectra were collected by the FTIR spectrometer (Bruker Vertex-80). X-ray photoelectron spectroscopy (XPS) measurements were extracted by theta probe X-ray photoelectron spectrometer (Thermo Fisher Scientific). As the x-ray source, the system uses a monochromated Al-Kα source with energy of 1486.6 eV. The spot diameter on the sample surface is 400 μm. For high-resolution (HR) scans, pass energy of 20 eV and an energy step size of 0.05 eV were used at the hemispherical analyzer. A dual flood gun which provides low-kinetic energy electrons and Ar^+ ions was used for charge compensation on the sample. Data acquisition and evaluation is performed via the Avantage software (Thermo Fisher Scientific). The smart background correction function in the Avantage software was used for background correction of HR-XPS spectra and is based on a modified Shirley background function. To correct charging, the binding energies of all spectra were referenced to the values of the $Pb4f_{7/2}$ binding energy of Pb(0) artifacts at 136.5 eV.[32]

Absorbance, transmittance, and reflectance of $MAPbI_3$ thin films with and without the DPP860 interface passivation layer were recorded by a UV-Vis-NIR spectrometer (Perkin Elmer Lambda 1050). Tungsten and deuterium lamps are used as a light source to provide a wide range of wavelength from 150 to 3100 nm. The surface morphology of the films was characterized by using Bruker Innova atomic force microscopy (AFM) and scanning electron microscopy (SEM). Photoluminescence spectra of sample films were measured using a Shamrock SR-303i monochromator and an Andor™ iDus Si-CCD detector. Samples were excited at 488 nm with 5 mW power using a COHERENT OBIS 488-150 LS laser. A set of long-pass filters was used to avoid any distortion of the recorded spectra by the laser light. Time-resolved photoluminescence measurements were performed using time-correlated single photon counting (TCSPC). The setup for TCSPC measurements consists of a DeltaNu DNS-300 monochromator (slit widths: 3 mm), a Becker & Hickl SPC 150 TCSPC module, and a PMC-100-1 photomultiplier. As an excitation light source, the setup uses a NKT Photonics SuperK FIANIUM FIU-15 with a pulse picker, connected to a Photon Etc LLTF Contrast VIS wavelength selection unit.

To characterize the photovoltaic (PV) performance of the perovskite solar cells photocurrent density-photovoltage (J-V) response was measured by using Keithley-2400-LV source meter. A LOT-QD solar simulator with a 1000 W xenon lamp providing AM1.5 global spectrum was used for irradiation. The intensity of the solar simulator was calibrated by the silicon reference

diode. The dark current density (JD)-voltage response of hole-only devices was measured using Keithley-2400-LV source meter to get the space-charge limited current (SCLC) curves.

The external-quantum efficiency (EQE) was measured by using an optical setup consisting of a lock-in amplifier (SR830; Stanford Research Systems) and a Jaissle 1002 potentiostat functioning as a preamplifier. Devices were illuminated with light from a xenon lamp passing through a monochromator (Oriel Cornerstone)). A filter wheel holding long-pass filters and a mechanical chopper were mounted between the xenon lamp and a monochromator with chopping frequencies in the range of 10-200 Hz was chosen. The silicon diode (Hamamatsu S2281) was used as a reference for the light intensity at each wavelength to calibrate in a range between 10 and 200 Hz.

Intensity-modulated photovoltage spectroscopy (IMVS) measurements were executed at V_{oc} conditions under illumination with 10% light-modulated amplitude to gain insight on the recombination dynamics in devices with and without DPP860 passivation. The parameters were set to measure the perturbed V_{oc} which is DC-voltage with 10% light intensity perturbation in the frequency range from 1 MHz to 50 mHz by using the PhotoEchem software. Then, the values of LED light intensity were set by the program to vary the intensity by controlling the current applied to the LED source.

3 | RESULTS AND DISCUSSION

3.1 | Chemical analysis

Infiltration of the moisture to the OIHP thin films has been pointed out as one of the extrinsic factors which degrade the photoactive layer.[33] To mitigate such problems, moisture-resistant molecules or polymers have been widely used as the interface passivators.[34] They also serve as the barrier for the either ion or electrode diffusion to the charge transporting or photoactive layers[35] We employed diketopyrrolopyrrole-based polymer (DPP860), as a ultra-thin layer between photoactive and PCBM layers (Figure 1A). To assess the degree of the hydrophobicity improvement, contact angle measurement was used for OIHP thin films with and without DPP860. The result shows that films covered with DPP860 exhibit higher contact angle than the pristine film, indicating the increment of hydrophobicity due to DPP860 treatment (Figure 1B). In addition to this, interface passivation may form interface dipoles which facilitate the injection of electrons by minimizing interface-induced nonradiative recombination.[11,36] Fourier transform infrared (FTIR) technique was used to study the existence and interaction of DPP860 on the surface of OIHP thin films. On this point, FTIR analysis (Figure 1C) reveals the formation of two new peaks at

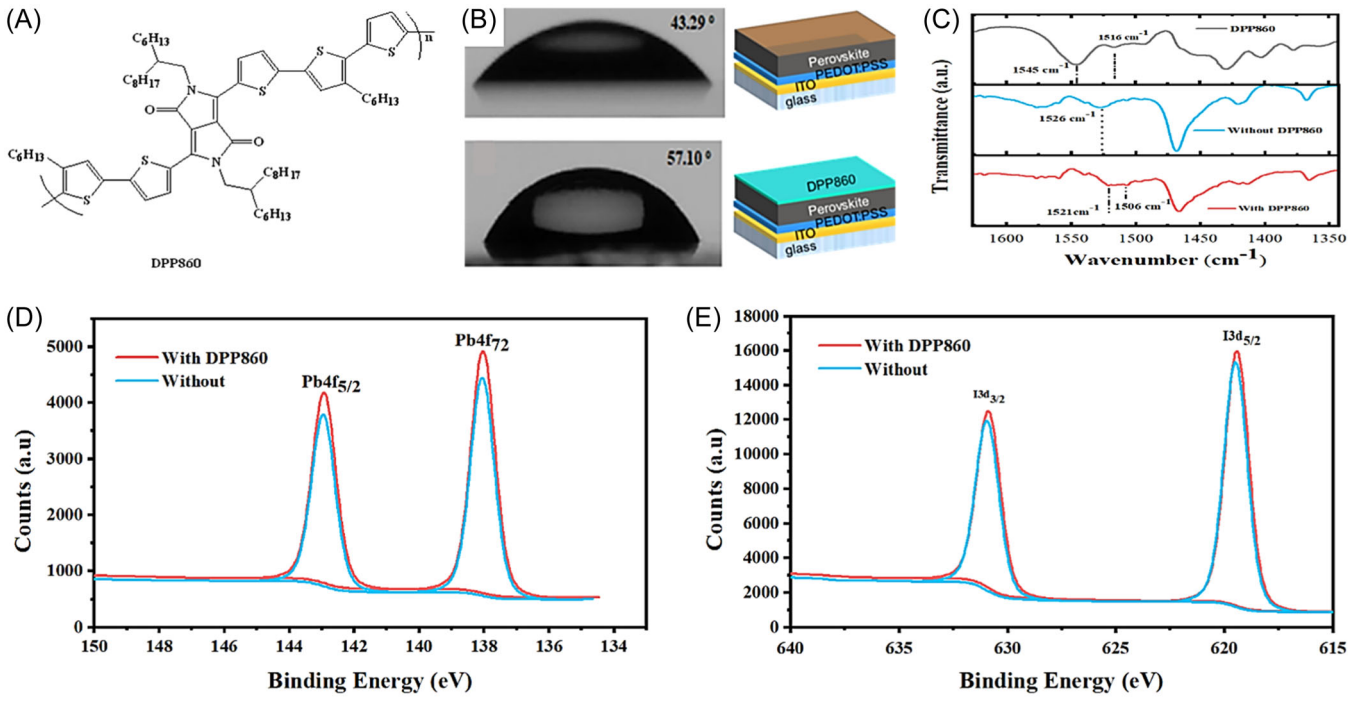

FIGURE 1 (A) Chemical structure of DPP860. (B) Contact angle measurement and schematic structure of perovskite films without (top) with DPP860 coating (bottom). (C) FTIR spectra and characteristic XPS peaks for (D) Pb4f and (E) I3d of perovskite films with and without DPP860 passivation.

1521 cm^{-1} (–C-N stretching) and 1506 cm^{-1} (N-H bending) when DPP860 is spin-coated on top of the HOIP thin films.[37] This shows that there is an interaction between OIHP thin films and the interface passivator, DPP860. XPS measurements were also carried out to investigate chemical interactions between OIHP thin films and DPP860. As it is shown in Figure 1D, XPS spectra do not show a notable shift in binding energy of Pb^{2+} which confirms the insignificant chemical interactions between functional groups of the interface passivating polymer and Pb^{2+}. But XPS spectra in Figure 1E shows that there is a slight shift to lower binding energy, which suggests the presence of chemical interactions between I^- and DPP860. Supporting Information S1: Figure S1a-f and Table S1 also show additional peaks of C1s, O1s and N1s and a change in peaks shape after DPP860 coated on top of the OIHP thin films. All findings from contact angle, FTIR, and XPS measurements prove that different types of interactions take place at the surface of the perovskite layer treated with the DPP860 passivator.

3.2 | Optoelectronic responses

Inverted planar OIHPSCs containing a capping layer, DPP860, between OIHP and phenyl-C61-butyric acid methyl ester (PCBM) layers were fabricated (Figure 2A). It is well-known that defected interfaces are serving as the trapping or recombination centers of charge carriers.[38] So it is important to have a proper energy level alignment along each interface as shown in Figure 2B to avoid trapping or recombination which affects the whole performance and affects the long-term stability of the OIHPSCs.[39,40] Regarding to this, the DPP860 which was known in the literature as electron donating polymer in organic solar cells, was used as the interface passivating thin layer in between the OIHP and PCBM layers to reduce the trapping or recombination rate. Moreover, it prevents ingression of moisture toward photoactive layer as the hydrophobic layer and insulation of metal electrode due to diffused halide ions.

UV-visible spectroscopy measurements were used to study the role of the DPP860 coating on the absorbance of the photoactive layer. The lowest transmittance spectrum is observed for OIHP films coated with DPP860 passivating layer (Figure 3A). In view of that, passivating the interface between PCBM and absorber layers could increase the photoabsorption. Likewise, the dark current of the OIHPSCs was recorded to extract current leakage, which is associated with the degree of charge trapping density in a device (Figure 3B). Various important electrical parameters, such as shunt resistance (Rsh) and ideality factor (n_{id}), of the OIHPSCs across the hetrojunction at low voltage can be extracted from this curve.[41,42] The obtained smaller leakage current of the passivated device assures that charge trap densities at the interface of $CH_3NH_3PbI_3$ and PCBM are reduced, which ascribes that nonradiative recombination is curtailed. Consequently, high Rsh, small dark currents and low n_{id} as a result of minimized defect density of the passivated device are vibrant variables to improve the current density (J_{sc}), fill factor (FF) and thus the PCE of the device.

Space-charge-limited current (SCLC) characteristics of hole-only devices having device structure of glass/ITO/PEDOT:PSS/$CH_3NH_3PbI_3$/poly(bis(4-phenyl)(2,4,6-trimethylphenyl)amine (PTAA)/Al and Glass/ITO/PEDOT:PSS/$CH_3NH_3PbI_3$/DPP860/PTAA/Al were assessed to compare the trap density (Figure 3C,D). The three regions: ohmic ($n = 1$), trap filled limited (TFL) ($n > 3$), and space charge limited current (SCLC) ($n = 2$) are indicated.[5,43] Accordingly, the onset voltage at which the

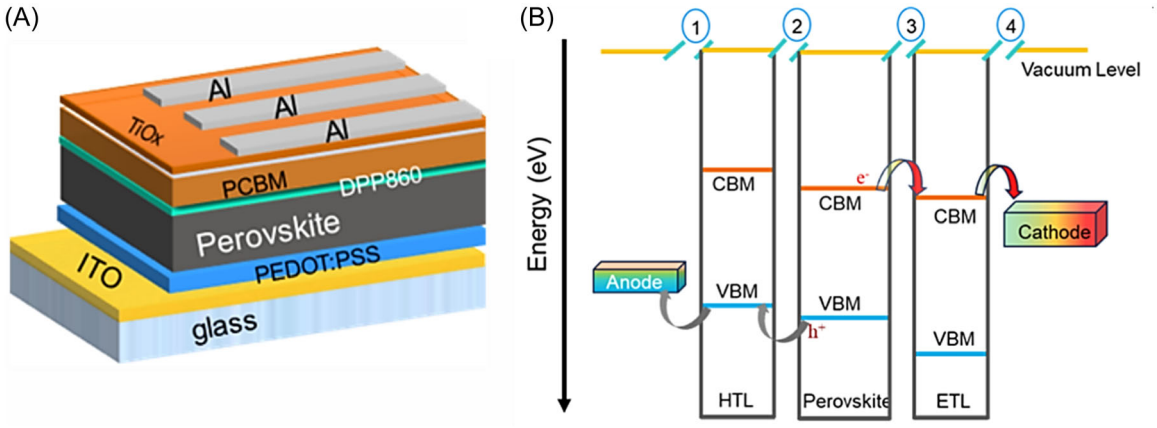

FIGURE 2 (A) schematics of passivated OIHPSCs with p-i-n configuration (B) Interfaces in p-i-n OIHPSCs (1) anode/HTL, (2) HTL/Perovskite, (3) Perovskite/ETL, and (4) ETL/Cathode.

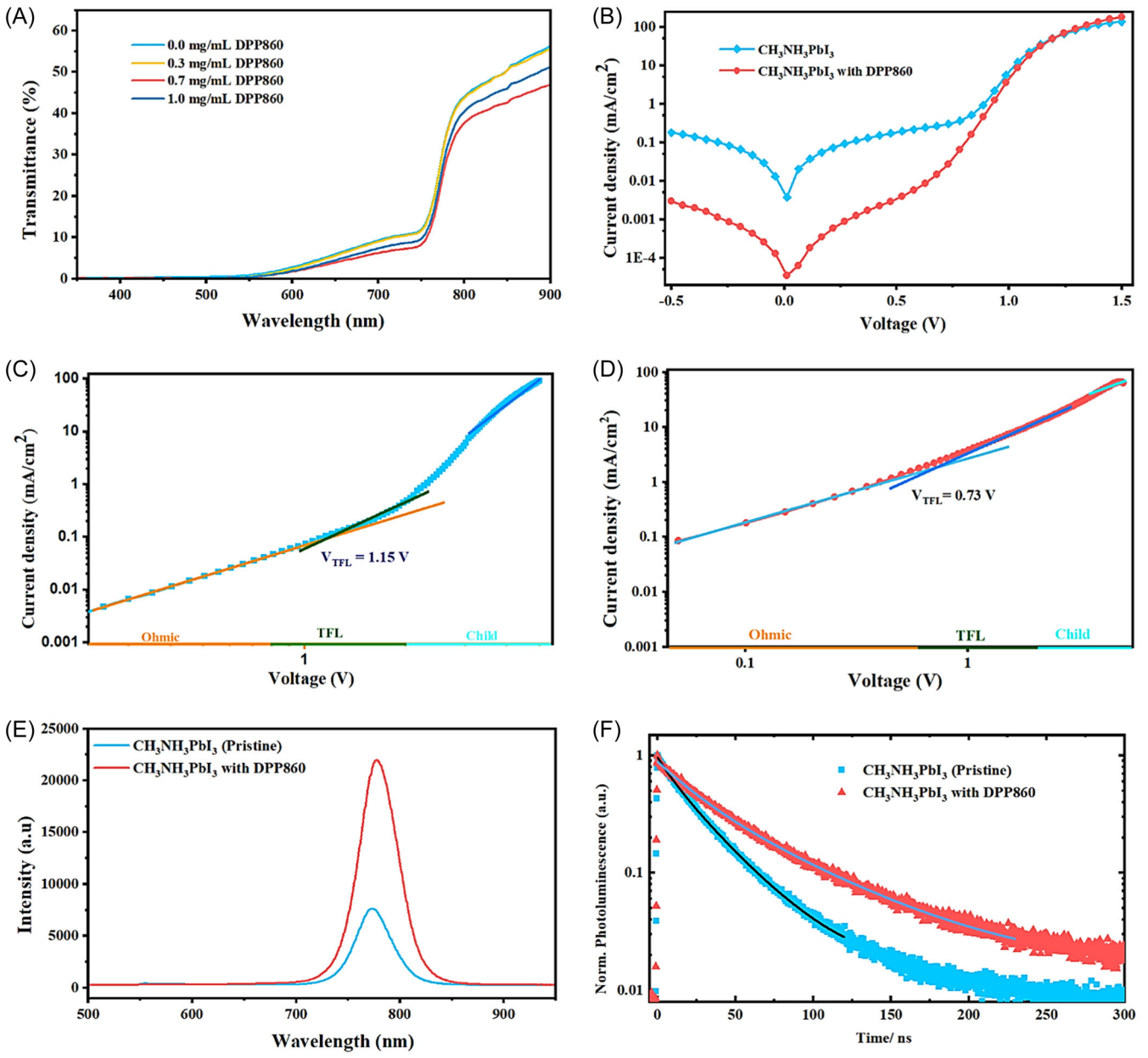

FIGURE 3 Optoelectronic response of $CH_3NH_3PbI_3$ perovskite with and without DPP860 passivation. (A) UV-Vis transmittance of perovskite films. (B) Semi-log plot of dark current density-voltage characteristics, and (C and D) space-charge-limited current (SCLC) of hole only device without and with DPP860, respectively. (E) Steady-state photoluminescence (PL), and (F) time-resolved photoluminescence (TRPL) spectra of films with and without DPP860 treatment.

traps are starting to fill by holes in the hole only devices with interface passivation exhibit a lower V_{TFL} of 0.73 V compared to 1.25 V for control devices. The trap density of the device is calculated using an equation,[44] ($n_t = (2\varepsilon_o \varepsilon V_{TFL}/eL^2)$, where ε_o is the vacuum permittivity constant, ε is the relative dielectric constant of MAPbI$_3$,[45] ($\varepsilon = 32.2$), e is the elementary charge and L the thickness of the photoactive layer. Quantitatively, devices without and with DPP860 passivator exhibit trap densities of ~1.47×10^{16} cm^{-3} and ~9.3×10^{15} cm^{-3}, respectively, indicating devices with passivators contain reduced defect density by one order. This could be attributed to the passivation of the defects across the interface. In other words, passivation enhances the efficiency of the hole extraction across the interface between $CH_3NH_3PbI_3$ and PCBM.

Based on the fundamental principle that a good solar cell is also a good light emitter,[46] the radiative emission processes of the OIHP were studied to explore the role of the DPP860 coating on the $CH_3NH_3PbI_3$ layer. Here,

three independent processes can ensue after photogenerated charge carriers are excited, viz. bimolecular (radiative) recombination, monomolecular (trap-assisted) recombination, and charge extraction.[47] Hence, low bimolecular and monomolecular recombination, and high charge extraction processes have yielded better performance for the OIHPSCs. To compare the degree of the monomolecular or bimolecular recombination process or charge extraction, photoluminescence properties of the different devices which have the glass/ITO/PEDOT:PSS/OIHP/and glass/ITO/PEDOT:PSS/OIHP/DPP860 structures were measured (Figure 3E). The steady-state photoluminescence spectra were measured by exciting samples with a 488 nm COHERENT OBIS 488-150 LS laser. The results show bimolecular (radiative) recombination processes are dominant in the structure which was interface passivated by DPP860. Interestingly, the results support that the amount of photogenerated electrons which could be injected to the PCBM may be increased after the excitation of electrons from DPP860 coated photoactive layer. The PL peak intensity increased for the corresponding films coated with 1.0, 0.3 and 0.7 concentrations (mg mL^{-1}) of DPP860, respectively (Supporting Information S1: Figure S2). Perovskite films coated with 0.7 mg mL^{-1} of passivator show the highest PL emission peak. On the contrary, it could be decreased for the mentioned concentrations due to quenching of photogenerated charge carried by PCBM. Thus, the aforementioned findings clearly signify that spin-coating DPP860 as the passivation layer on top of the $CH_3NH_3PbI_3$ layer decreases the strength of bimolecular and monomolecular recombination processes while more photogenerated charge carriers are extracted by PCBM.[48] Moreover, the results strengthen that DPP860 effectively passivates interfacial defects at the interface between $CH_3NH_3PbI_3$ and PCBM.

Additionally, time-resolved photoluminescence data were also collected to find out the impact of thin layer of DPP860 as an interface passivator in reducing nonradiative recombination (Figure 3F).[49] The data of the TRPL curves are well fitted with a bi-exponential decay equation of $f(t) = A_1\exp(-t/\tau_1) + A_2\exp(-t/\tau_2) + B$, where τ_1 and τ_2 are the decay time constants, while A_1 and A_2 are the corresponding decay amplitudes and B is a constant for the base-line offset.[50] The average decay time constant τ_{avg} was calculated according to Equation (1). τ_1 and τ_2 are strongly related to the monomolecular (trap-assisted) recombination and bimolecular (radiative) recombination, respectively.[51,52] With respect to τ_1, Figure 3F and Table 1 substantiate that it is longer for the interface passivated films, attributes to the low trap assisted recombination. Similarly, longer slow decay life time (τ_2) for 0.7 mg mL^{-1} DPP860 coated photoactive layer is related to bimolecular recombination which ascribes the production of more photogenerated charge carriers from the $CH_3NH_3PbI_3$ layer.[51] Moreover, the average decay lifetime results (Table 1) reveal that trap-assisted recombination processes are less dominant in DPP860-coated films compared to the control device. The findings of the TRPL investigation are compellingly consistent with the steady-state photoluminescence spectra. Furthermore, topographic morphology analysis using atomic force microscope (AFM) and scanning electron microscopy (SFM) confirms that the changes in morphology due to DPP860 passivation is insignificant (Supporting Information S1: Supplementary note-1 and Figure S3).

TABLE 1 Summary of time constants extracted from time-resolved photoluminescence spectra of perovskite films coated with and without DPP860 polymer.

DPP860 concentration (mg mL^{-1})	A_1	A_2	τ_1 (ns)	τ_2 (ns)	τ_{avg} (ns)
0.0	0.24	0.71	10.5	30.1	28.1
0.3	0.23	0.68	11.6	35.2	32.9
0.7	0.39	0.48	22.3	62.7	53.6
1.0	0.20	0.68	8.6	33.1	31.4

$$\tau_{avg} = \frac{A_1\tau_1^2 + A_2\tau_2^2}{A_1\tau_1 + A_2\tau_2}. \quad (1)$$

3.3 | PV responses characterization

It is well known that the extraction of photogenerated charge carriers are strongly affected by the defect density of the interface between the cathode/electron transport layer (ETL), ETL/photoactive layer, hole transport layer (HTL)/photoactive layer, and anode/HTL.[53,54] In particular, the interfaces between ETL/photoactive layer and HTL/photoactive layer are determinant in enhancing injection of the charge carriers and yielding better photovoltaic parameters.[55,56]

To scrutinize the role of DPP860 interface passivation on enhancing photovoltaic properties, current density-voltage (J-V) characteristics of devices with and without passivator were measured under AM 1.5 G (100 mW cm^{-2}) solar spectrum illumination (Figure 4A). Different solutions of DPP860 concentrations 0.0, 0.3, 0.7, or 1.0 mg mL^{-1} were applied to find the optimal concentration which passivates interface defects using J-V characteristics. The J-V findings clearly show that incorporation of the DPP860 boosts the short current density (J_{sc}) and FF of the OIHPSCs which

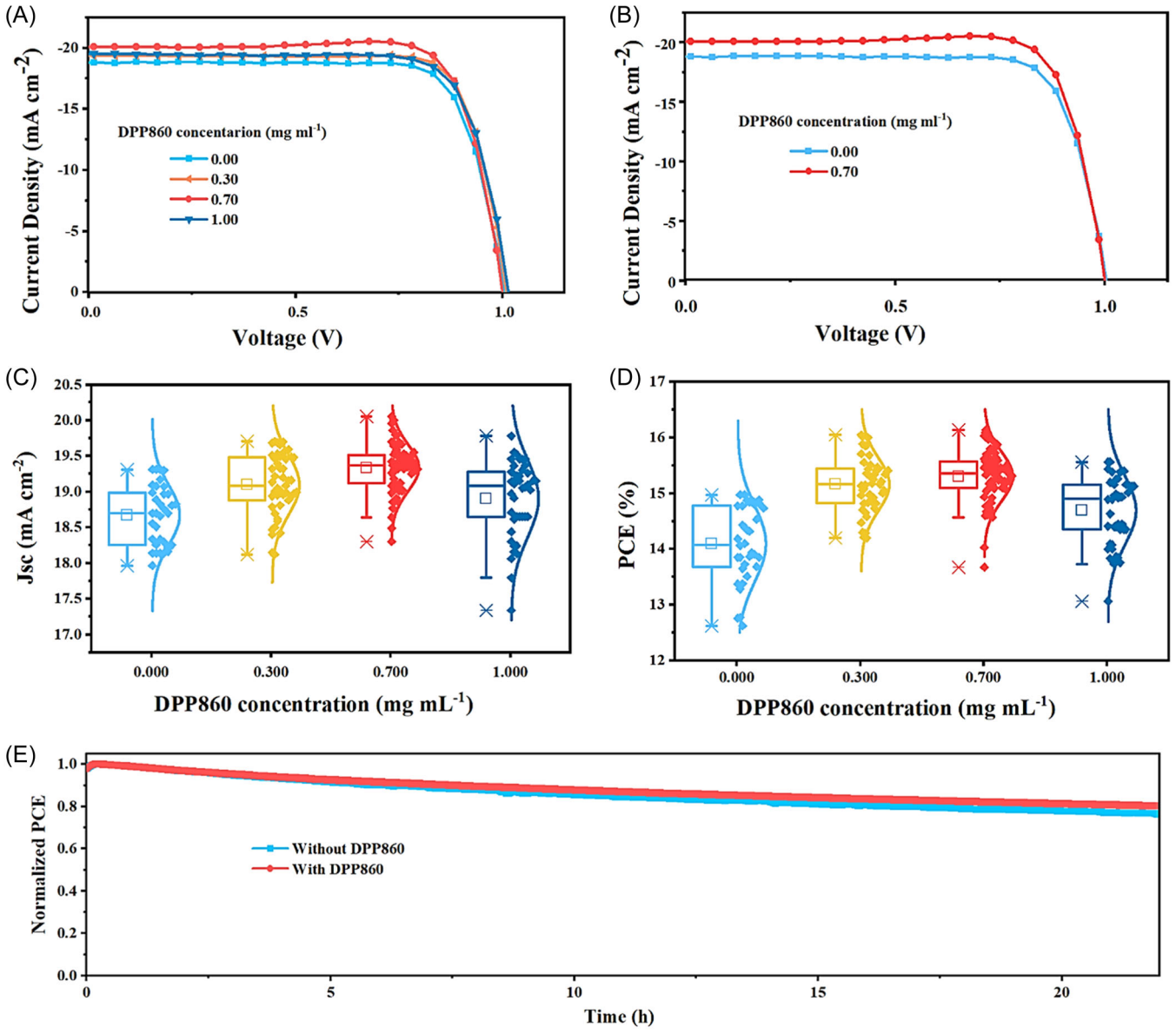

FIGURE 4 Photovoltaic properties of perovskite devices with and without DPP860 passivation. (A) J-V curves of the devices treated with 0.0, 0.3, 0.7, and 1.0 mg mL^{-1} DPP860. (B) J-V curves of perovskite solar cells treated with 0.0 and 0.7 mg mL^{-1} (the optimal concentration) DPP860. Statistical distribution of (C) short-circuit current density (J_{sc}), and (D) power conversion efficiency (PCE) of perovskite devices treated with 0.0, 0.3, 0.7, and 1.0 mg mL^{-1} DPP860. (E) Operational stability of encapsulated perovskite devices obtained from MPP tracking measurements under 1 sun (100 mW cm^{-2}) illumination.

ascribes to minimized trap-assisted and bimolecular recombination processes across the interface.[57] Devices treated with 0.7 mg mL^{-1} of DPP860 exhibit the optimum J_{sc} and FF and hence the highest average PCE of 15.2 ± 0.4% (Figure 4B). Subsequently, statistical distributions have been shown (Figure 4C,D) and (Supporting Information S1: Figure S4a,b) to compare the J_{sc}, PCE, V_{oc} and FF of the 62 and 30 devices with and without DPP860, respectively. The average and best PV properties that correspond to the statistical distribution are also indicated in Table 2. Moreover, the measured external quantum efficiency (EQE) spectra of the passivated OIHPSC show relative improvement in EQE and the integrated short circuit current density (Supporting Information S1: Figure S5a). Maximum power point tracking (MPPT) technique was used to study the operational stability of the devices with and without DPP860 interface passivation under continuous photoirradiation (100 mW cm^{-2}, AM1.5 G). Devices with passivation interlayer display improved stability compared to control devices (Figure 4E).

TABLE 2 Summary of photovoltaic parameters obtained from J-V characteristics of perovskite devices treated with DPP860 interface passivator of various concentrations.

Concentration (mg mL^{-1})		V_{oc} (V)	J_{sc} (mA cm^{-2})	FF (%)	PCE (%)
0.0	Av.	0.99 ± 0.02	18.7 ± 0.41	76.27 ± 2.11	14.09 ± 0.68
	Best	1.00	18.8	78.8	14.9
0.3	Av.	1.00 ± 0.01	19.17 ± 0.38	77.80 ± 1.45	14.93 ± 0.41
	Best	1.01	19.4	79.3	15.7
0.7	Av.	1.00 ± 0.02	19.30 ± 0.33	78.61 ± 1.68	15.21 ± 0.43
	Best	1.00	20.1	79.7	16.0
1.0	Av.	1.00 ± 0.01	18.93 ± 0.57	77.74 ± 1.39	14.69 ± 0.66
	Best	1.01	19.7	79.2	15.8

Abbreviations: FF, fill factor; PCE, power conversion efficiency.

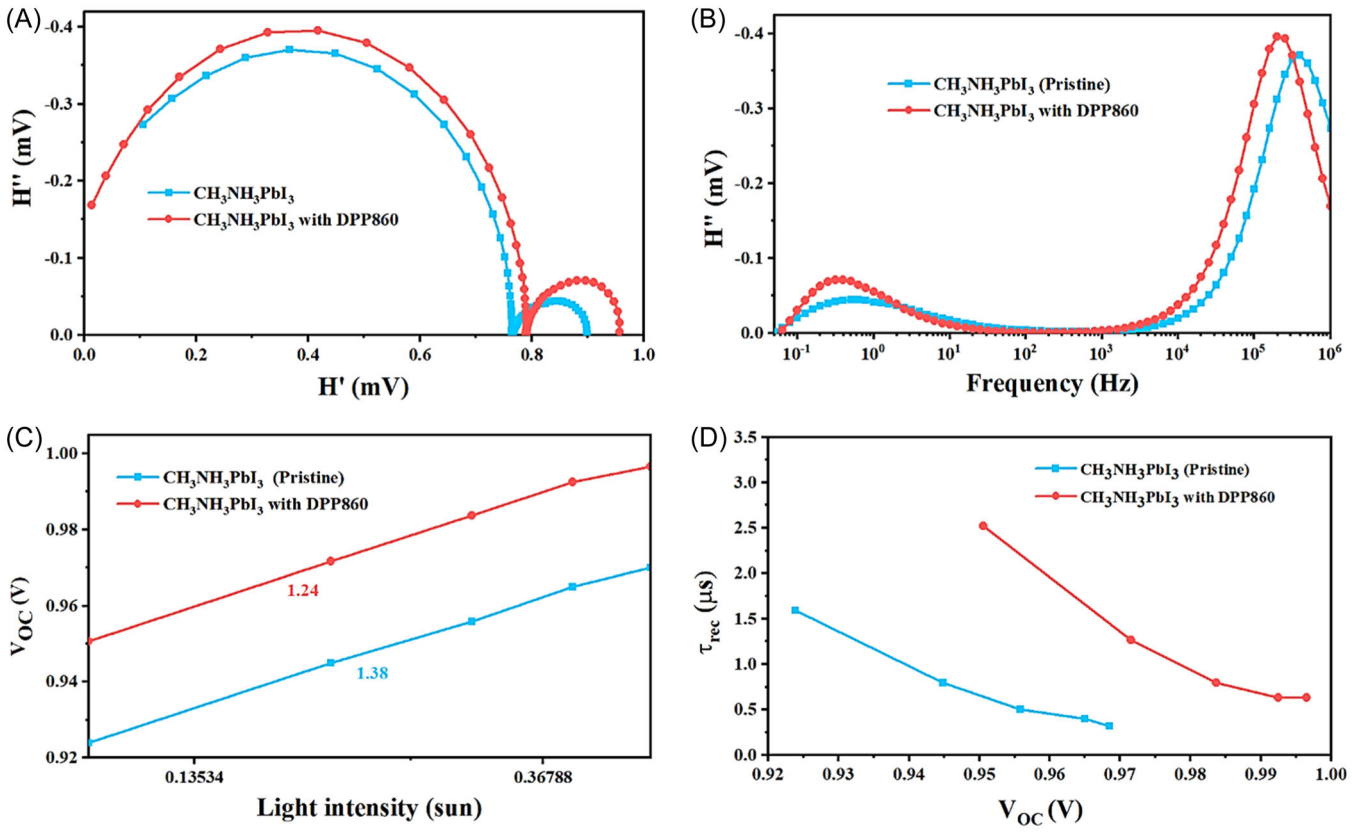

FIGURE 5 Intensity-modulated photovoltage characteristics of $MAPbI_3$ PSCs containing 0.0 and 0.7 (mg mL^{-1}) of DPP860. (A) Nyquist plots, (B) Imaginary transfer function (H'') versus frequency plots, (C) open-circuit voltage (V_{oc}) as a function of photon flux (cm^{-2} s^{-1}) intensity, and (D) charge carrier recombination time constant (τ_{rec}) as a function of the V_{oc} of OIHPSCs.

The depletion of the J_{sc} and FF was noteworthy for control and passivated devices after irradiance, though the relative change in Voc is insignificant (Supporting Information S1: Figure S5b). This suggests that the incorporation of the DPP860 as the interface passivator improves the operational stability of the OIHPSCs.

3.4 | Charge carrier recombination dynamics

Intensity-modulated photovoltage spectroscopy (IMVS) was used to scrutinize the impact of DPP860 in reducing the charge carrier recombination dynamics in OIHPSCs.

Measurement results were recorded in the absence of charge extraction (at open-circuit) to find the decay of charge carriers as a result of defects in OIHPSCs. In IMVS response, the dominant SRH recombination (recombination resistance) phenomena are mainly observed in the lower transfer function (high-frequency region) of the Nyquist plot (Figure 5A), which is analogous to a lower frequency in electrochemical impedance spectroscopy (EIS) results.[58] The findings show that devices with DPP860 exhibit enhanced recombination resistance compared to the reference device (device without DPP860).

Figure 5B presents the imaginary transfer function (H'') versus frequency, which was scanned in the range of 1 MHz to 50 mHz under 8 mW cm^{-2} LED light illumination with 10% light intensity modulation. The critical frequency (f_c) ($f_c = \frac{1}{2\pi\tau_c}$), which is directly related to the maximum of H'' at high frequency and inversely proportional to the time constant (τ_c) was determined. Results show that devices with DPP860 exhibit longer time constant compared to those without, which suggests a lower charge recombination rate in interface passivated devices.[59] Moreover, the ideality factor (n_{id}), which is calculated from the slope of the graph of V_{oc} as a function of light illumination intensity (Figure 5C), suggests the presence of trap-assisted recombination in the devices.[60] The extracted n_{id} for the OIHPSCs with 0.7 mg mL^{-1} and without DPP860 are ~1.24 and ~1.38, respectively. The results infer that the improved V_{oc} of treated OIHPSCs is attributed to the reduced trap-assisted recombination and high shunt resistance of devices.[61]

The recombination time-constant versus light illumination intensity graph (Figure 5D) was plotted to compare the recombination time-constant of OIHPSCs with and without interface passivation. Devices with DPP860 show a longer recombination lifetime compared to devices without, which is ascribed to the suppressed trap-assisted recombination and improved charge extraction processes across devices interface.

4 | CONCLUSIONS

The findings in this work unveil that interface passivation using DPP860 has the potential to minimize nonradiative recombination at the interface between OIHP and PCBM. Thus, it facilitates the injection of charge carriers and their mobility across the interface. On the other hand, it also improves the hydrophobicity of the light absorbing layer and alleviates problems regarding moisture ingression to the perovskite layer from ETL side. Moreover, the interface-passivated p-i-n OIHPSCs that were processed in an ambient environment disclosed significant improvements, particularly in J_{sc}, FF, and stability compared to control devices. The results confirm that interface passivation using DPP860 is an optional strategy to reduce trap-assisted recombination and improve the overall performance of $MAPbI_3$-based perovskite solar cells.

ACKNOWLEDGMENTS

We would like to acknowledge Erasmus+ KA107 (project number 2020-1-AT01-KA107-077800), Linz Institute for Organic Solar cells (LIOS), Johannes Kepeler University, Linz, Africa Uni-net and OeAD-GmbH – Austria's Agency for Education and Internationalization, Addis Ababa Science and Technology University, Hawassa University for their financial, materials and laboratory support.

CONFLICT OF INTEREST STATEMENT

The authors declare no conflict of interest.

ORCID

Getachew Adam Workneh http://orcid.org/0000-0002-2863-1379

REFERENCES

1. National renewable Energy Laboratory (NREL). *Best Research-Cell Efficiencies*. National renewable Energy Laboratory (NREL); 2023.
2. Kaltenbrunner M, Adam G, Głowacki ED, et al. Flexible high power-per-weight perovskite solar cells with chromium oxide-metal contacts for improved stability in air. *Nat Mater*. 2015;14:1032-1039. doi:10.1038/nmat4388
3. Ponseca CS, Savenije TJ, Abdellah M, et al. Organometal halide perovskite solar cell materials rationalized: ultrafast charge generation, high and microsecond-long balanced mobilities, and slow recombination. *J Am Chem Soc*. 2014;136:5189-5192. doi:10.1021/ja412583t
4. Comin R, Walters G, Thibau ES, Voznyy O, Lu ZH, Sargent EH. Structural, optical, and electronic studies of wide-bandgap lead halide perovskites. *J Mater Chem C*. 2015;3:8839-8843. doi:10.1039/c5tc01718a
5. Shi D, Adinolfi V, Comin R, et al. Low trap-state density and long carrier diffusion in organolead trihalide perovskite single crystals. *Science*. 2015;347:519-522. doi:10.1126/science.aaa2725
6. Tombe S, Adam G, Heilbrunner H, et al. The influence of perovskite precursor composition on the morphology and photovoltaic performance of mixed halide $MAPbI_{3-x}Cl_x$ solar cells. *Sol Energy*. 2018;163:215-223. doi:10.1016/j.solener.2018.01.083
7. Abicho S, Hailegnaw B, Workneh GA, Yohannes T. Role of additives and surface passivation on the performance of perovskite solar cells. *Mater Renew Sustain Energy*. 2022;11:47-70. doi:10.1007/s40243-021-00206-9

8. Zhou H, Chen Q, Li G, et al. Interface engineering of highly efficient perovskite solar cells. *Science*. 2014;345:542-546. doi:10.1126/science.1254050
9. Xiao M, Huang F, Huang W, et al. A fast deposition-crystallization procedure for highly efficient lead iodide perovskite thin-film solar cells. *Angew Chem Int Ed*. 2014;53:9898-9903. doi:10.1002/anie.201405334
10. Mohamad Noh MF, Arzaee NA, Safaei J, et al. Eliminating oxygen vacancies in SnO2 films via aerosol-assisted chemical vapour deposition for perovskite solar cells and photoelectrochemical cells. *J Alloys Compd*. 2019;773:997-1008. doi:10.1016/j.jallcom.2018.09.273
11. Ye F, Zhang S, Warby J, et al. Overcoming C60-induced interfacial recombination in inverted perovskite solar cells by electron-transporting carborane. *Nat Commun*. 2022;13:7454. doi:10.1038/s41467-022-34203-x
12. Dai J, Xiong J, Liu N, et al. Synergistic dual-interface modification strategy for highly reproducible and efficient PTAA-based inverted perovskite solar cells. *Chem Eng J*. 2023;453:139988. doi:10.1016/j.cej.2022.139988
13. Song J, Wang L, Cui Q, et al. Interface passivation of perovskite solar cells by Fmoc-Ala-OH amino acids. *J Electron Mater*. 2023;52:2303-2311. doi:10.1007/s11664-023-10265-5
14. Duan C, Zhang X, Du Z, et al. Perovskite interface defect passivation with poly (ethylene oxide) for improving power conversion efficiency of the inverted solar cells. *Opt Express*. 2023;31:20364-20376.
15. Nishihara Y, Onozawa-Komatsuzaki N, Zou X, Marumoto K, Chikamatsu M, Yoshida Y. Effect of passivation on the interface between perovskite and donor–acceptor copolymer-based hole-transport layer in perovskite solar cells. *Chem Lett*. 2020;49:1341-1344. doi:10.1246/cl.200497
16. Wang F, Zhang Y, Yang M, et al. Interface dipole induced field-effect passivation for achieving 21.7% efficiency and stable perovskite solar cells. *Adv Funct Mater*. 2021;31:1-10. doi:10.1002/adfm.202008052
17. Liu M, Dahlström S, Ahläng C, et al. Beyond hydrophobicity: how F4-TCNQ doping of the hole transport material improves stability of mesoporous triple-cation perovskite solar cells. *J Mater Chem A*. 2022;10:11721-11731. doi:10.1039/d2ta02588d
18. Mei D, Qiu L, Chen L, et al. Incorporating polyvinyl pyrrolidone in Green anti-solvent isopropanol: a facile approach to obtain high efficient and stable perovskite solar cells. *Thin Solid Films*. 2022;752:139196. doi:10.1016/j.tsf.2022.139196
19. Yang S, Ma W, Zhang Z, et al. Inverted perovskite solar cells based on inorganic hole transport material of $CuInS_2$ with high efficiency and stability. *Sol Energy*. 2021;230:485-491. doi:10.1016/j.solener.2021.10.040
20. Zheng R, Zhao S, Zhang H, et al. Defect passivation grain boundaries using 3-aminopropyltrimethoxysilane for highly efficient and stable perovskite solar cells. *Sol Energy*. 2021;224:472-479. doi:10.1016/j.solener.2021.06.001
21. Deng X, Cao Z, Yuan Y, et al. Coordination modulated crystallization and defect passivation in high quality perovskite film for efficient solar cells. *Coord Chem Rev*. 2020;420:213408. doi:10.1016/j.ccr.2020.213408
22. Wang S, Zhang Z, Tang Z, et al. Polymer strategies for high-efficiency and stable perovskite solar cells. *Nano Energy*. 2021;82:105712. doi:10.1016/j.nanoen.2020.105712
23. Chen W, Shi Y, Wang Y, et al. N-type conjugated polymer as efficient electron transport layer for planar inverted perovskite solar cells with power conversion efficiency of 20.86%. *Nano Energy*. 2020;68:104363. doi:10.1016/j.nanoen.2019.104363
24. Wojciechowski K, Leijtens T, Siprova S, et al. C60 as an efficient n-type compact layer in perovskite solar cells. *J Phys Chem Lett*. 2015;6:2399-2405. doi:10.1021/acs.jpclett.5b00902
25. Choi DS, Kwon SN, Na SI. Non-fullerene small molecule electron-transporting materials for efficient p-i-n perovskite solar cells. *Nanomaterials*. 2020;10:1082.
26. Ripolles-Sanchis T, Raga SR, Guerrero A, et al. Molecular electronic coupling controls charge recombination kinetics in organic solar cells of low bandgap diketopyrrolopyrrole, carbazole, and thiophene polymers. *J Phys Chem C*. 2013;117:8719-8726. doi:10.1021/jp402751v
27. Burschka J, Pellet N, Moon SJ, et al. Sequential deposition as a route to high-performance perovskite-sensitized solar cells. *Nature*. 2013;499:316-319. doi:10.1038/nature12340
28. Park SH, Roy A, Beaupré S, et al. Bulk heterojunction solar cells with internal quantum efficiency approaching 100%. *Nat Photonics*. 2009;3:297-302. doi:10.1038/nphoton.2009.69
29. Adam G, Kaltenbrunner M, Głowacki ED, et al. Solution processed perovskite solar cells using highly conductive PEDOT:PSS interfacial layer. *Sol Energy Mater Sol Cells*. 2016;157:318-325. doi:10.1016/j.solmat.2016.05.011
30. Hailegnaw B, Adam G, Wielend D, Pedarnig JD, Sariciftci NS, Scharber MC. Acetylacetone improves the performance of mixed halide perovskite solar cells. *J Phys Chem C*. 2019;123:23807-23816. doi:10.1021/acs.jpcc.9b05058
31. Ouyang J, Xu Q, Chu CW, Yang Y, Li G, Shinar J. On the mechanism of conductivity enhancement in poly(3,4- ethylenedioxythiophene):poly(styrene sulfonate) film through solvent treatment. *Polymer*. 2004;45:8443-8450. doi:10.1016/j.polymer.2004.10.001
32. McGettrick JD, Hooper K, Pockett A, et al. Sources of Pb(0) artefacts during XPS analysis of lead halide perovskites. *Mater Lett*. 2019;251:98-101. doi:10.1016/j.matlet.2019.04.081
33. Ma Z, Xiao Z, Zhou W, et al. Efficient $CH_3NH_3PbI_{3-x}(SeCN)_x$ perovskite solar cells with improved crystallization and defect passivation. *J Alloys Compd*. 2020;822:153539. doi:10.1016/j.jallcom.2019.153539
34. He Q, Worku M, Xu L, et al. Surface passivation of perovskite thin films by phosphonium halides for efficient and stable solar cells. *J Mater Chem A*. 2020;8:2039-2046. doi:10.1039/c9ta12597c
35. Boyd CC, Cheacharoen R, Bush KA, Prasanna R, Leijtens T, McGehee MD. Barrier design to prevent metal-induced degradation and improve thermal stability in perovskite solar cells. *ACS Energy Lett*. 2018;3:1772-1778. doi:10.1021/acsenergylett.8b00926
36. Hu L, Zhang L, Ren W, et al. High efficiency perovskite solar cells with PTAA hole transport layer enabled by PMMA: F4-TCNQ buried interface layer †. *J Mater Chem C*. 2022;10:9714-9722. doi:10.1039/d2tc01494g
37. Karakus G, Polat ZA, Yenidunya AF, Zengin HB, Karakus CB. Synthesis, characterization and cytotoxicity of novel modified

poly[(maleic anhydride)- co-(vinyl acetate)]/noradrenaline conjugate. *Polym Int*. 2013;62:492-500. doi:10.1002/pi.4341
38. Ball JM, Petrozza A. Defects in perovskite-halides and their effects in solar cells. *Nat Energy*. 2016;1:16149. doi:10.1038/nenergy.2016.149
39. Tang J, Tian W, Zhao C, et al. Imaging the moisture-induced degradation process of 2D organolead halide perovskites. *ACS Omega*. 2022;7:10365-10371. doi:10.1021/acsomega.1c06989
40. Hailegnaw B, Adam G, Heilbrunner H, et al. Inverted (p-i-n) perovskite solar cells using a low temperature processed TiO_x interlayer. *RSC Adv*. 2018;8:24836-24846. doi:10.1039/c8ra03993c
41. Tvingstedt K, Gil-Escrig L, Momblona C, et al. Removing leakage and surface recombination in planar perovskite solar cells. *ACS Energy Lett*. 2017;2:424-430. doi:10.1021/acsenergylett.6b00719
42. Wang Q, Shao Y, Dong Q, Xiao Z, Yuan Y, Huang J. Large fill-factor bilayer iodine perovskite solar cells fabricated by a low-temperature solution-process. *Energy Environ Sci*. 2014;7:2359-2365. doi:10.1039/c4ee00233d
43. Jain SC, Kapoor AK, Geens W, Poortmans J, Mertens R, Willander M. Trap filled limit of conducting organic materials. *J Appl Phys*. 2002;92:3752-3754. doi:10.1063/1.1503863
44. Bube RH. Trap density determination by space-charge-limited currents. *J Appl Phys*. 1962;33:1733-1737. doi:10.1063/1.1728818
45. Li J, Hua X, Gao F, et al. Green antisolvent additive engineering to improve the performance of perovskite solar cells. *J Energy Chem*. 2022;66:1-8. doi:10.1016/j.jechem.2021.06.023
46. Wehrenfennig C, Liu M, Snaith HJ, Johnston MB, Herz LM. Homogeneous emission line broadening in the organo lead halide perovskite $CH_3NH_3PbI_{3-x}Cl_x$. *J Phys Chem Lett*. 2014;5:1300-1306. doi:10.1021/jz500434p
47. Zhang H, Qiao X, Shen Y, Wang M. Effect of temperature on the efficiency of organometallic perovskite solar cells. *J Energy Chem*. 2015;24:729-735. doi:10.1016/j.jechem.2015.10.007
48. Hong J, Kim H, Hwang I. Defect site engineering for charge recombination and stability via polymer surfactant incorporation with an ultra-small amount in perovskite solar cells. *Org Electron*. 2019;73:87-93. doi:10.1016/j.orgel.2019.06.003
49. Yamada Y, Endo M, Wakamiya A, Kanemitsu Y. Spontaneous defect annihilation in CH3NH3PbI3 thin films at room temperature revealed by time-resolved photoluminescence spectroscopy. *J Phys Chem Lett*. 2015;6:482-486. doi:10.1021/jz5026596
50. Mao H, Huang Y, Ma Z, et al. Surface grain boundary passivation via mixed antisolvent and PC 61 BM assistant for stable perovskite solar cells. *J Mater Sci: Mater Electron*. 2019;30:3511-3520. doi:10.1007/s10854-018-00628-8
51. Xi J, Xi K, Sadhanala A, et al. Chemical sintering reduced grain boundary defects for stable planar perovskite solar cells. *Nano Energy*. 2019;56:741-750. doi:10.1016/j.nanoen.2018.11.021
52. Zhang K, Liu Z, Wang N. Highly efficient inverted ternary organic solar cells with polymer fullerene-free acceptor as a third component material. *J Power Sources*. 2019;413:391-398. doi:10.1016/j.jpowsour.2018.12.073
53. Li X, Sheng W, Duan X, et al. Defect passivation effect of chemical groups on perovskite solar cells. *ACS Appl Mater Interfaces*. 2022;14:34161-34170. doi:10.1021/acsasmai.1c08539
54. Guo Z, Xue T, Sun X, et al. Activate whole-body passivation ability of small isomeric D-π-A molecules via amino position effect to improve the photovoltaic performance of perovskite solar cells. *Chem Eng J*. 2023;452:139321. doi:10.1016/j.cej.2022.139321
55. Kim GW, Min J, Park T, Petrozza A. Defect passivation through (α-methylguanido)acetic acid in perovskite solar cell for high operational stability. *ACS Appl Mater Interfaces*. 2022;14:20848-20855. doi:10.1021/acsami.2c00231
56. Kim GW, Min J, Park T, Petrozza A. Bulk passivation and interfacial passivation for perovskite solar cells: which one is more effective? *Adv Mater Interfaces*. 2021;8:2002078. doi:10.1021/acsami.2c00231
57. Chen J, Park NG. Materials and methods for interface engineering toward stable and efficient perovskite solar cells. *ACS Energy Lett*. 2020;5:2742-2786. doi:10.1021/acsenergylett.0c01240
58. Shariatinia Z. Recent progress in development of diverse kinds of hole transport materials for the perovskite solar cells: a review. *Renew Sustain Energy Rev*. 2020;119:109608. doi:10.1016/j.rser.2019.109608
59. Pockett A, Eperon GE, Sakai N, Snaith HJ, Peter LM, Cameron PJ. Microseconds, milliseconds and seconds: deconvoluting the dynamic behaviour of planar perovskite solar cells. *Phys Chem Chem Phys*. 2017;19:5959-5970. doi:10.1039/c6cp08424a
60. Caprioglio P, Wolff CM, Sandberg OJ, et al. On the origin of the ideality factor in perovskite solar cells. *Adv Energy Mater*. 2020;10:2000502. doi:10.1002/aenm.202000502
61. Choi J, Kamaraj E, Park H, et al. Defect-passivation of organometal trihalide perovskite with functionalized organic small molecule for enhanced device performance and stability. *Dyes Pigm*. 2021;189:109255. doi:10.1016/j.dyepig.2021.109255

SUPPORTING INFORMATION

Additional supporting information can be found online in the Supporting Information section at the end of this article.

How to cite this article: Abicho S, Hailegnaw B, Mayr F, et al. Interface passivation using diketopyrrolopyrrole-oligothiophene copolymer to improve the performance of perovskite solar cells. *Energy Sci Eng*. 2024;12:2272-2283. doi:10.1002/ese3.1745